intensified volcanism and enhanced ocean connectivity
Cretaceous Oceanic Anoxic Event 2 (OAE2) 94.5 million years ago

Yong-Xiang Li[1]*, Xinyu Liu[1], David Selby[2,3], Zhonghui Liu[4], Isabel P. Montañez[5], Xianghui Li[1]

[1.] State Key Laboratory for Mineral Deposits Research, Key Laboratory of Surficial Geochemistry, Ministry of Education, School of Earth Sciences and Engineering, Nanjing University, Nanjing 210046, China

[2.] Department of Earth Sciences, University of Durham, Durham, DH1 3LE, UK

[3] State Key Laboratory of Geological Processes and Mineral Resources, China University of Geosciences, Wuhan 430074, China

[4] Department of Earth Science, The University of Hong Kong, Hong Kong, China

[5] Department of Earth and Planetary Sciences, University of California, Davis, CA 95616, USA

Corresponding author, Email: yxli@nju.edu.cn

Abstract

Oceanic anoxic event 2 (OAE2) exemplifies an episode of global oceanographic and climatic changes in the mid-Cretaceous greenhouse, primarily documented in stratigraphically condensed sections in the Northern Hemisphere. However, the timing and mechanism of its global initiation remain elusive. Here we report a high-resolution initial osmium isotope ($^{187}Os/^{188}Os_i$, Os_i) and $\delta^{13}C_{org}$ record from a substantially expanded OAE2 interval in southern Tibet, China that was then deposited in the Southern Hemisphere. The record documents episodic, intensifying volcanism with the highest intensity episode marked by a large Osi excursion at ~94.5 Ma and a subsequent ~200 kyr Osi minimum concomitant with a cooling interval, which is broadly synchronous with the Plenus Cold Event recorded in the Northern Hemisphere. Paradoxically, the large Osi excursion lags the onset of OAE2 by ~50 kyr and occurred during a globally near synchronous transgression. These results demonstrate that, besides volcanism, enhanced ocean connectivity may have played a critical role in triggering the global onset of OAE2 at ~94.5 Ma.

Keywords: Cenomanian-Turonian Boundary, Osmium isotopes, carbon cycle, southern Tibet, transgression, Mid-Cretaceous greenhouse

Introduction

Oceanic Anoxic Event 2 (OAE2) occurred during the latest Cenomanian and the earliest Turonian (Cenomanian-Turonian Boundary - CTB, ~93.9 Ma) (Meyers et al., 2012; Jones et al., 2020) and exemplifies one of the most pronounced episodes of ocean-wide anoxia in the mid-Cretaceous greenhouse world (e.g., Schlanger and Jenkyns, 1976; Jenkyns, 2010; Owens et al., 2013; Jenkyns et al., 2017). Dramatic changes in ocean conditions during OAE2 are manifested by the widespread deposition of organic-rich sediments in major ocean basins, rapid marine biotic turnover, pronounced positive carbon isotope excursions (CIEs) in both organic matter and carbonates, and other distinct geochemical anomalies (e.g., S, Li, Hg, Os, and Cr isotopes) (e.g., Jenkyns, 2010; Gomes et al., 2016; Jenkyns et al., 2017; Clarkson et al., 2018). The coeval CIEs archived in the terrestrial records (e.g., Wu et al., 2009; Barclay et al., 2010; Takashima et al., 2011) as well as the accompanying accelerated hydrological cycling and enhanced weathering of continental silicate rocks (Blätter et al., 2011; Pogge von Strandmann et al., 2013) attest to the global nature of OAE2 and signify the wholesale dramatic changes of the Earth system during one of the warmest periods of the planet.

OAE2 provides a prime example of global change in a deep-time greenhouse world when numerous anomalous environmental processes occurred likely involving a cascade of environmental tipping points being crossed. One of the enduring efforts is to unravel the global initiation of OAE2 by disentangling leads/lags of these various geological processes to elucidate the causal links and feedbacks associated with the onset of OAE2. Submarine magmatism/volcanism has long been speculated to have triggered OAE2 (e.g., Larson, 1991; Bralower, 2008). Yet, direct dating of submarine volcanism proves to be difficult as ages obtained directly from lavas often possess uncertainties too large to establish a definitive causal link to a magmatic source. Although the Caribbean large igneous province (LIP) is often considered to be the source of volcanism (e.g., Snow et al., 2005), magmatism associated with other LIPs such as the High Arctic LIP or HALIP (e.g., Tegner et al., 2011), the Kerguelen Plateau (e.g., Leckie et al., 2002), and younger pulses of the Ontong Java Plateau (e.g., Mahoney et al., 1993) are also considered possible candidates.

Osmium (Os) isotopes provide an indirect means of deciphering submarine volcanism in marine successions. Osmium isotopes of marine strata are shown to preserve seawater osmium isotope compositions that largely reflect mixing of two endmember Os isotope components: a submarine volcanism related unradiogenic Os isotopic composition ($^{187}Os/^{188}Os$ = 0.127) and a continental weathering related more radiogenic Os isotopic composition ($^{187}Os/^{188}Os$ = 1.4). Os isotope values near the $^{187}Os/^{188}Os$ ratio of 0.127 are commonly referred to as unradiogenic and values greater than 0.127 and closer to the modern seawater $^{187}Os/^{188}Os$ ratio of 1.06 are generally referred to as radiogenic (e.g., Sullivan et al., 2020). The short residence time of Os isotopes in the ocean (≤10 kyr) (Oxburgh, 2001; Rooney et al., 2016) allows for geologically rapid changes to be recorded in the Os isotopic composition of ocean water and preserved in marine sediments. A prominent shift from relatively radiogenic to unradiogenic Os isotope values prior to the onset of OAE2, together with elevated Os concentration, was first reported for the OAE2 interval from the Demerara Rise (equatorial Proto-North Atlantic) and observed in the OAE2 interval from central Italy (western Tethys seaway) (Turgeon and Creaser, 2008). Comparable pronounced Os isotope shifts were subsequently reported from other OAE2 intervals including the Western Interior Seaway (WIS) of the North America, European epicontinental sea, Southern Atlantic, and the Pacific Ocean (Du Vivier et al., 2014; 2015), indicating widespread presence of a magmatic signature proximal to OAE2.

While a shift to unradiogenic $^{187}Os/^{188}Os$ compositions in several sedimentary successions provides compelling evidence for widespread volcanic influence, the occurrence of a negative Os isotope excursion at a given site is also related to the ocean circulation patterns that transmit the volcanic Os signature from the LIP source to the depositional site. Thus, the phasing relationship between a large shift to unradiogenic $^{187}Os/^{188}Os$ and the onset of OAE2 at geographically disparate sites holds key insight into the global initiation of OAE2. Deconvolving this insight, however, has been limited to date given multiple issues. First, the phasing relationship has not been well defined in many OAE2 sections reflecting that some OAE2 intervals are stratigraphically condensed, typically only a few meters thick or less (e.g., Tsikos et al., 2004). Stratigraphic condensation prevents sampling at adequate temporal resolutions for both carbon and osmium isotope records. Second, the first issue is further exacerbated by the presence of sedimentary hiatus at the base of some OAE2 intervals (e.g., Gambacorta et al., 2015; Eldrett et al., 2017; Jones et al., 2020). Third, studies have been typically focused on the positive CIEs of OAE2, thus stratigraphic intervals below the positive CIEs of OAE2 in many existing carbon isotope records (e.g., the Furlo section, central Italy; Jenkyns et al., 2007; Turgeon and Creaser, 2008) are insufficiently sampled prohibiting detailed examination of the phasing relationship.

Fourth, despite OAE2 being considered a global event, the knowledge of OAE2 is primarily based on records from the Northern Hemisphere, particularly the proto-North Atlantic realm (e.g., Tsikos et al., 2004; Sageman et al., 2006; Elrick et al., 2009; Wang et al., 2011; Jenkyns et al., 2017; Kuhnt et al., 2017). Existing OAE2 Os records are predominantly from the Northern Hemisphere (Turgeon and Creaser, 2008; Du Vivier et al., 2014, 2015; Schoder-Adams et al., 2019; Sullivan et al., 2020; Percival et al., 2020) with a single Os record from the Southern Atlantic (ODP Site 530) in the Southern Hemisphere (Du Vivier et al., 2014). Although ODP Site 530 also documents an Os isotopic shift at the onset of OAE2 (Du Vivier et al., 2014), the OAE2 interval at ODP Site 530 is incomplete due to poor core recovery, hampering a detailed understanding of the OAE2 at this Southern Hemisphere site. And lastly, even for OAE2 sections of high-resolution sampling, a high-resolution chronological timescale required for quantitative assessment of the phasing relationship between volcanism, ocean circulation, and the initiation of OAE2 is lacking for many OAE2 sections.

Here, we report, for one of the most globally expanded OAE2 intervals, a high-resolution osmium stratigraphy of the Gongzha section, southern Tibet, which was paleogeographically situated in the eastern Tethys Ocean in the Southern Hemisphere (Fig. 1, SM1). This section is temporally constrained by a high-resolution astrochronologic timescale that is anchored to the well-constrained CTB (93.95 ± 0.05 Ma, Meyers et al., 2012; Jones et al., 2020; Fig. S1-1) of the GSSP section in Western Interior Seaway (WIS). In addition, to complement the existing high-resolution carbonate $\delta^{13}C_{carb}$ record, which documents the most detailed and complete carbon isotope variations during OAE2 (Li et al., 2017), we also present a high-resolution $\delta^{13}C_{org}$ record for this Tibetan section to further interrogate the carbon cycle dynamics during OAE2 in the Southern Hemisphere, for which OAE2 records remain scarce.

Results

$\delta^{13}C_{org}$ isotope stratigraphy

The $\delta^{13}C_{org}$ values of the Gongzha section vary between -25.7‰ and -21.9‰ and display a broad positive CIE interval from 36.7 m to 72.6 m (Fig. 2d; Table 1), which is almost identical to the OAE2 interval previously defined using the $\delta^{13}C_{carb}$ data (Fig. 2c). $\delta^{13}C_{org}$ values in the CIE interval also delineate a stepwise perturbation, plateau, and recovery stages that are broadly consistent with corresponding Stages C3, C4 and C5 defined by the $\delta^{13}C_{carb}$ data (Figs. 2c, 2d). The stepwise perturbation also shows details of the 1st buildup, the trough, and the 2nd buildup substages comparable with those of the $\delta^{13}C_{carb}$ data. The $\delta^{13}C_{org}$ data show two enrichment intervals that straddle the $\delta^{13}C_{carb}$ peak (Figs. 2c, 2d). Also, the $\delta^{13}C_{org}$ plateau appears dampened and slightly narrower in comparison to the plateau of Stage C4 in the $\delta^{13}C_{carb}$ record (Figs. 2c, 2d). Overall, the $\delta^{13}C_{org}$ data exhibit a variation pattern largely resembling that of the $\delta^{13}C_{carb}$ data (Figs. 2c, 2d), and corroborate the previous definition of the CIE of the Gongzha section (Li et al., 2017).

The difference ($\Delta^{13}C$) between paired $\delta^{13}C_{carb}$ and $\delta^{13}C_{org}$ values from the Gongzha defines a broad interval of multiple $\Delta^{13}C$ minima (Fig. 2e). This interval straddles the C3/C4 boundary and spans ~1.2 short eccentricity cycles (Fig. 2b), representing ~120 kyr, as constrained by the orbital timescale developed for this section (Li et al., 2017). The $\Delta^{13}C$ values further show elevated values in the upper part of Stages C4 and C5 and remain high above the CIE interval (Fig. 2e).

Osmium isotope data

The Re abundance of the studied interval varies from ~0.15 to 2.5 ppb (Table 2), which is similar to that observed in other OAE2 intervals (Turgeon and Creaser, 2008;

Du Vivier et al., 2014, 2015; Schoder-Adams et al., 2019; Jones et al., 2020). The ^{192}Os abundance, reflecting the hydrogenous (seawater-derived) Os component, ranges from ~30 to 360 ppt (Table 2) with two horizons exhibiting elevated abundances at 40.8 m and 47.4 m (Fig. 2g).

The initial $^{187}Os/^{188}Os$ (Osi) values are calculated using the $^{187}Re/^{188}Os$ and $^{187}Os/^{188}Os$ measured isotope compositions (Table 2) at 94 Ma. The Osi compositions vary between ~0.15 and 0.85 (Fig. 2f). The osmium isotope record exhibits three distinct stepwise Osi shifts to increasingly lower values with increasingly higher magnitudes of change at 13.8 m, 26 m, and 40 m (Fig. 2f). Based on the chronology of the section (Li et al., 2017), these three Osi shifts occurred at 94.5±0.15 Ma, 94.8±0.15 Ma, and 95.1±0.15 Ma, respectively (Fig. 2f). The minor Osi shift (~0.1) at ~95.1 Ma and the moderate Osi shift (~0.3) at ~94.8 Ma are followed by a gradual return to broadly background radiogenic values of ~0.75-0.84, whereas the large Osi excursion (>0.5) at ~94.5 Ma is followed by an interval of sustained low Osi values of ~0.15 prior to a gradual return toward relatively radiogenic values of 0.6-0.7 (Fig. 2f). The large negative Osi excursion at ~94.5 Ma spans a ~1.2 m thick interval, representing about 30 kyr. The subsequent interval of minimum Osi values comprises nearly 2 short eccentricity cycles, thus lasting for ~200 kyr (Fig. 2b, 2f), and exhibits two ^{192}Os concentration peaks (Fig. 2g). A subtle small increase in ^{192}Os concentration of a few 10s ppt accompanies the moderate Osi shift at ~94.8 Ma (Fig. 2g). In contrast, no obvious change in ^{192}Os abundance occurs synchronously with the minor Osi shift at ~95.1 Ma.

Comparison of Osi and the CIE in the Gongzha section

The most striking feature is that the large negative Osi excursion at ~94.5 Ma occurs *after* the onset of the Stage C3 C isotope perturbation (i.e., the onset of OAE2) that is preceded by background Stage C1 and Stage C2 of a brief minor negative $\delta^{13}C$ shift (Li et al., 2017) (Fig. 2). Therefore, the large Osi excursion at ~94.5 Ma occurs after the onset of OAE2 (Fig. 2). Based on astronomic temporal constraints (Li et al., 2017), the large Osi excursion lags the onset of OAE2 by ~50 kyr. Moreover, the interval of minimum Osi values following the large negative Osi excursion persists for ~200 kyr and occurs *within* the Stage C3 unfolding of the positive CIE (Fig. 2). Specifically, the interval of the negative Osi excursion straddles the "trough" substage C3b (Fig. 2). The moderate Osi excursion at ~94.8 Ma and the possible minor Osi excursion at ~95.1 Ma occur ~250 kyr and ~550 kyr *prior* to the onset of OAE2, respectively (Fig. 2).

Discussion and Implications

The highly expanded OAE2 interval in the Tibetan Gongzha section documents one of the most complete and detailed CIE of OAE2 and has been correlated with other major OAE2 sections in the northern Hemisphere using a proposed carbon isotope stage scheme (Li et al., 2017), which is comparable to other correlation schemes (SM2). Among the other OAE2 sections, the CTB GSSP sections in the Western Interior Seaway (WIS), North America and the Yezo Group section (YG), Japan are unique. The CTB GSSP sections of the WIS were deposited in an epicontinental sea, which developed in western North America, and are constrained by well-resolved chronologies. The Yezo Group section archives OAE2 in an open ocean setting in the western Pacific and contains a highly expanded OAE2 interval. New radiometric age data for the Yezo Group section (Du Vivier et al., 2015) permit refinement of the carbon isotope stages of OAE2 in this section (SM3, Fig. S3-1). Relatively more expanded OAE2 intervals in WIS have been identified recently and can be also well correlated (Jones et al., 2019, 2020; Sullivan et al., 2020), and carbon isotope stages in the most expanded OAE2 interval documented to date, the Iona-1 core from the WIS, are readily recognized (SM4). Based on this information, we propose a high-resolution correlation of the Osi and $\delta^{13}C$ records for the OAE2 interval archived in the Gongzha Tibetan section (this study), the Portland core CTB GSSP, the Iona-1 core of WIS, and the YG section in Japan using a carbon isotope stage correlation scheme (Fig. 3).

1) Episodic, successively intensifying volcanism

The Osi record from the significantly expanded OAE2 interval of the Gongzha

Tibetan section, eastern Tethys Ocean, provide the first high-resolution Osi stratigraphy for the Southern Hemisphere. The minor, moderate, large Osi excursions at ~95.1 Ma, ~94.8 Ma, and ~94.5 Ma, respectively, probably indicate three episodes of increasingly intensified volcanism (Fig. 2f). Given that the Gongzha section was situated in an open ocean setting, the Osi excursions likely record a global signature of volcanism. Indeed, the large Osi excursion at ~94.5 Ma corresponds to the distinct Osi excursions documented in several other OAE2 sections (e.g., Du Vivier et al., 2014, 2015; Schoder et al., 2019; Jones et al., 2020). Particularly, it can be correlated with the large Osi excursion (at 0 m) recorded in the Portland Core, WIS, and with the Osi excursion (at -19.3 m) in the YG section, Japan (Du Vivier et al., 2014, 2015; Jones et al., 2020) (Fig. 3). This correlation is also supported by similar ages estimated independently from each section. The large Osi excursion in the Portland Core (Du Vivier et al., 2014) occurs about 5.5 short eccentricity cycles below the CTB (Meyers et al., 2012; Jones et al., 2020) and can thus be constrained to ~94.5 ± 0.05 Ma, an age that is also in agreement with the age-depth model for the WIS location (Du Vivier et al., 2015) and a subsequent age model revision (Jones et al., 2020). The large Osi excursion in the YG section occurs immediately below a volcanic bed dated at 94.44±0.14 Ma (Du Vivier et al., 2015). Similarly, the interval of minimum Osi values in the Tibetan section corresponds in age to comparable Osi minima in the aforementioned sections with OAE2 records (Du Vivier et al., 2014, 2015), specifically, the 0-~1.5 m interval of Portland Core (WIS) and the -19.3 m to -5 m interval of the YG (Fig. 3). This interval in the Tibetan section exhibits two ^{192}Os peaks and represents ~200 kyr, which is strikingly similar to that of the Portland Core, which also exhibits two ^{192}Os peaks (Du Vivier et al., 2014) that span nearly 2 short eccentricity cycles, i.e., ~200 kyr (Fig. 3). In the equivalent interval in the YG section, only one ^{192}Os peak is defined, possibly due to low sampling resolution in this highly expanded YG section (Du Vivier et al., 2015). In essence, the episode of most intensified volcanism that started at ~94.5 Ma and persisted for ~200 kyr is widely documented in different geological settings and in geographically distant sections, arguing for a global fingerprint of intense volcanism. This feature also implies that the world oceans were well connected at this time and that the Os signature of volcanism was distributed rapidly (10-30 kyrs) across the globe via ocean circulation.

In the Tibetan section, the earlier moderate Osi excursion constrained to ~94.8 Ma resembles a comparable excursion (at -5.0 m) in the Portland Core as well as in YG section (at ~-65 m) (Fig. 3). This proposed correlation is strengthened by the accompanying subtle increase in ^{192}Os abundance in all three sections (Fig. 3) and their similar inferred ages (Du Vivier et al., 2015). Intriguingly, in the expanded OAE2 interval of the Iona-1 core (WIS), the large Osi excursion (at ~111.5 m) is dated at ~94.8 Ma (Fig. 3). The subsequent interval of minimum Osi values in the Iona-1 core is stratigraphically thicker, temporally much longer, and exhibits more ^{192}Os peaks (Sullivan et al., 2020) than the correlated interval in the Portland core or in other OAE2 sections (Fig. 3). In essence, these data indicate that there was an episode of strong volcanism at ~94.8 Ma that left a distinct fingerprint in the Iona-1 core site of WIS and moderate, but strikingly comparable signatures in other regions globally.

The correlation of the OAE2 intervals between the two WIS cores have been established previously (e.g., Eldrett et al., 2015, 2017; Sullivan et al., 2020; Jones et al., 2020; Fig. S4-1, S4-2). In this study (Fig. 3) we propose an alternative correlation by integrating the additional constraints of the newly reported Os isotope record from the Iona-1 core (Sullivan et al., 2020) and re-analysis of the CIE interval in the Iona-1 core using the carbon-isotope-stage correlation scheme previously defined for the Tibetan section (Li et al., 2017). Our objective was to correlate the OAE2 record of the stratigraphically expanded Iona-1 core with those of other OAE2 sections using the same carbon-isotope-stage correlation scheme (SM4). The alternative correlation model was defined utilizing: (1) the common feature of the Osi profiles in the two WIS cores, that is, a transition from the Osi minimum interval to the subsequent gradual Osi shift toward relatively radiogenic Osi values; (2) the band-passed short eccentricity (E2) orbital timescales of the two WIS cores (Meyers et al., 2012; Eldrett et al., 2015) (Fig. S4-3a). With this correlation, the ages for the OAE2 interval in the Iona-1 core can be straightforwardly extracted from the very well-constrained CTB age for the Portland core GSSP (Fig. S4-3a) and thus do not depend on the numerical age model for the

Iona-1 core (Eldrett et al., 2015). This is important as the age model of Eldrett et al. (2015) has relatively large uncertainties and has been proposed by Jones et al. (2020) to yield biased older ages (Jones et al., 2020). The new proposed correlation is largely in line with previous stratigraphic correlations of the two cores by Eldrett et al (2015, 2017) and Sullivan et al (2020), despite differing stratigraphic definitions of CIE intervals in these previous studies. In this process we defined carbon isotope stages for the CIE interval in the Iona-1 core that in turn permits distinction of the globally correlative portion (Stages C3-C4-C5) from the previously defined, but regional portion of the CIE referred to as Stage C3a' (Fig 3; Fig. S4-3b).

The resulting durations of the stages of the global CIE are in excellent agreement with those of the substantially expanded OAE2 interval of the Gongzha section, southern Tibet (Table S4-1). The regional CIE is broadly equivalent to an interval encompassing the precursor to CIE events of Eldrett et al. (2015). Therefore, the total CIE interval recorded in the Iona-1 core (Fig. 3) that consists of both the 'regional CIE' and the subsequent 'global CIE' yields a longer OAE2 duration estimate than that inferred for many other OAE2 sections (SM4, Fig. S4-3b, Table S4-2). Our proposed alternative correlation is also different from the recent correlation of the two WIS cores by Jones et al (2020), in which the CIE interval of the Iona-1 core was re-defined by alignment of the large Osi excursions in the two cores (Fig. S4-2). This was based on an implicit assumption that the large Osi excursions must be synchronous in the two cores. While the duration of the CIE interval of the Iona-1 core as redefined by Jones et al. (2020) correlates very well with that of the Portland core, the duration of the prominent Osi minimum in the Iona-1 core is much longer than that of the comparable minimum interval in the Portland core (Fig. S4-2). Conversely, if the thicker Osi minimum interval of the Iona-1 core were a result of high sedimentation rates, the duration of the re-defined CIE interval would become much shorter than that of the Portland core (Fig. S4-2), revealing a mismatch in either scenario. Notably, the termination of the carbon isotope 'plateau' stage (C4) was placed at ~96.5 m in the re-defined CIE interval (Fig. 5 of Jones et al. 2020), which is below the stratigraphic level of the CTB (94.34-94.64 m) in the Iona-1 core (Eldrett et al., 2015). This is inconsistent with several other OAE2 sections, including two WIS cores, the Portland and SH#1 cores, for which the termination of the carbon isotope 'plateau' is defined at or slightly above the CTB (Tsikos et al. 2004; Sageman et al., 2006; Jones et al., 2019). Given these inconsistencies, the OAE2 correlation of the Portland and Iona-1 cores established by Jones et al (2020) was not adopted in this study.

2) Restricted oceans at the eve (~94.8-94.5 Ma) of the global onset of OAE2

The Os isotope records from several OAE2 sections archive an episode of volcanism at ~94.8 Ma as a negative Osi excursion. This excursion, which is marked in the Iona-1 core, is followed by a prolonged interval of low Osi values, but by moderate and brief Osi excursions at other sites (Fig. 3), exhibiting regional differences in how this episode of volcanism was recorded. While an Osi excursion provides direct evidence of volcanism in a sedimentary record, geographically, the extent to which an Osi anomaly can be distributed from the LIP source through the global oceans is also influenced by the degree of connectivity between ocean basins and the efficiency of ocean circulation. The regional differences in how the episode of volcanism at ~94.8 Ma is recorded in the Osi records indicate that world oceans were not fully connected at that time and probably remained so until ~94.5 Ma when the global onset of the OAE2 took place. This may further indicate that the Iona-1 core was likely situated closer to the source of LIP volcanism than the other sites. The Iona-1 core, located in the southern WIS, was well connected to the proto-North Atlantic Ocean. During the Cenomanian, the proto-North Atlantic Ocean was in the course of opening and the proto-North Atlantic basin was substantially smaller than present-day and surrounded by land masses and shallow seaways connecting it with the eastern Tethys and the Pacific Ocean (Fig. 1) (e.g., Hay, 2008). Thus, it is reasonable to infer that the intermediate and deep water masses of the proto-North Atlantic basin were largely restricted. Submarine volcanism associated with the Caribbean LIP at ~94.8 Ma could have introduced abundant unradiogenic Os isotopes into the intermediate and deep water of the restricted proto-North Atlantic basin, resulting in a large Osi excursion at the Iona-1 core site. We hypothesize that a temporary surge in sea level during the magmatic episode at 94.8 Ma, followed by thermal subsidence of submarine volcanoes in the proto-North Atlantic Ocean could have temporarily created enhanced global ocean connectivity that permitted widespread distribution of the LIP-induced unradiogenic Os$_i$ signature. In turn, this would have given rise to a moderate and brief Os$_i$ excursion in further inland or distal regions from the source such as the shallow water setting of the WIS (the Portland core) and the more open ocean settings of the eastern Tethys (the Tibetan section) and western Pacific Ocean (the YG section), respectively (Fig. 3).

The magmatic episode at ~94.8 Ma not only caused a large Os$_i$ shift in the radiogenic Os composition of intermediate and deep waters, but could have contributed to the anoxia that developed in the restricted proto-North Atlantic Ocean. Anoxia led to burial of organic matter and in this region is recorded by a stepwise series of small positive CIEs, referred to as Stage C3a' that we refer to as the 'regional component of the CIE' in this study in comparison to the globally correlative CIEs of several OAE2 sections with good chronology control (Fig. 3, SM4, Fig. S4-3b). Stage C3a' started at ~94.7 Ma and ended at ~94.5 Ma (Fig. 3; Fig. S4-3b), probably indicating a subsequent ~200 kyr of anoxia and associated burial of organic matter in the restricted proto-North Atlantic Ocean.

3) Global onset of OAE2 at ~94.5 Ma: intensified volcanism, widespread transgression, and enhanced ocean connectivity

Intensified volcanism is indicated by a major Os$_i$ excursion at ~94.5 Ma in geographically distant OAE2 sections with good age control such as the Portland core, and the Tibetan and the YG sections (Fig. 3). Perhaps the most prominent and enigmatic feature in the OAE2 interval of the Tibetan section is that the episode of volcanism at ~94.5 Ma occurred ~50 kyr *after* the onset of the CIE (Figs. 2, 3). Such a 'lag' phase relationship is also documented in the highly expanded OAE2 interval of the YG section, Japan (Fig. 3; SM3, Fig. S3-1c). Both the Tibetan and the YG sections were situated in open ocean settings, but one in the Southern Hemisphere and the other in the Northern Hemisphere, respectively. Therefore, the 'lag' phasing relationship documented in the two sections should represent a genuine global signature. However, this 'lag' phasing is paradoxical because the positive CIE in the OAE2 interval has long been interpreted as recording increased burial of organic matter triggered by volcanism (e.g., Arthur et al., 1980; Turgeon and Creaser, 2008). In contrast, volcanism 'leading' or contemporaneous with the onset of OAE2 has been inferred from other records primarily from condensed sections in the proto-North Atlantic, western Tethys, and the WIS of North America (Turgeon and Creaser, 2008; Du Vivier et al., 2014, 2015; Jones et al., 2020). For example, the onset of OAE2 is constrained to ~60 kyr after the large Osi excursion at some inland WIS sites (Jones et al., 2020). Thus, the disparate phasing relationship in different regions presents a conundrum as to how OAE2 was initiated globally.

While the most intense volcanism at ~94.5 Ma introduced additional substantial unradiogenic Os isotopes, presumably continuation of the proto-North Atlantic Ocean source, the global record of this strong Os isotopic signature of volcanism (Fig. 3) can be explained by a eustatic rise in tandem with this episode of intense volcanism. Sea level rise would have connected the world ocean basins, allowing the signature of volcanism that was previously largely restricted in the proto-North Atlantic Ocean to be distributed to the global oceans, as evidenced by the globally similar Osi profiles from ~94.5 Ma onwards (Fig. 3).

The high-resolution Osi record from the open ocean Tibetan section indicates that this large Osi excursion occurs over an ~1.2 m stratigraphic interval, which corresponds ~30 kyr duration. This suggests efficient ocean circulation at that time and a residence time for Osi of less than 30 kyr, making it an effective proxy for interrogating rapid changes in ocean conditions in the deep time. The 'lag' phase relationships documented in the Tibetan and the YG sections (Fig. 3) show that the large Osi excursion (~94.5 Ma) postdated the onset of the buildup of the protracted positive carbon isotope excursion (~94.55 Ma).

The eustatic rise would have facilitated the rapid expansion of the deep-water volcanic Os signature to shallow depths. The major Osi excursion in the CTB GSSP interval (WIS) coincides with a transgressive surface, which can be broadly correlated around the proto-North Atlantic basin (Fig. 4) (e.g., Voigt et al., 2006; Gale et al., 2008; Navarro-Ramirez et al., 2016; Beil et al., 2018). The transgression was likely associated with a late Cenomanian sea level rise (Ce5, Haq, 2014) of 22 to 30 m (Voigt et al., 2006; Richardt et al., 2013). In the proto-North Atlantic basin, it is feasible that a transgression of this magnitude and supplied with increased volcanic-sourced nutrients could have induced enhanced burial of organic matter and the positive CIE in the basin. In turn, this would create a 'leading' phase relationship in records from this region. For instance, in the SH#1 core (WIS), the large Osi excursion coincides with a boundary of lithological change from limestone to sandy mudstone (~122.5 m), indicative of transgression, and that precedes the onset of the CIE (~121 m) (Fig. 5 of Jones et al., 2020).

Regardless of the phasing relationship between the large Osi excursion and the onset of CIE of OAE2 at any of the given sites, the aforementioned correlation of the OAE2 records requires that, besides volcanism, increased ocean connectivity created by a eustatic rise at ~94.5 Ma must have played a critical role in triggering the *global* onset of OAE2. Had no transgression or high sea level stands taken place at ~94.5 Ma, volcanism alone would have probably led to anoxia restricted to the proto-North Atlantic Ocean, analogous to that inferred for the earlier episode of volcanism at ~94.8 Ma (e.g., as recorded by the Iona-1 core Osi record), assuming that other boundary conditions were comparable at ~94.8 Ma and ~94.5 Ma. While intense volcanism and global sea level rise at ~94.5 Ma were likely mechanistically related during LIP formation (Arthur et al., 1987), the profound importance of enhanced ocean connectivity in initiating *global* OAE2 is revealed by this study.

4) Globally well-connected oceans (~94.5 Ma onward): persistent volcanism, global C cycle perturbation, and bihemispheric cooling

The pronounced Osi excursion at ~94.5 Ma was followed by an interval of Osi minimum values that lasted for ~200 kyr and appears to record at least two pulses of volcanism (Sullivan et al., 2020; Jones et al., 2020; Fig. 3). The high-resolution Osi and carbon isotope data from the highly expanded Tibetan section in the Southern

Hemisphere documents that this interval ends slightly before the most enriched $\delta^{13}C$ values of the CIE are reached at the C3/C4 boundary (Figs. 2, 3). A similar feature is also exhibited by other OAE2 sections (Fig. 3) in the Northern Hemisphere (e.g., Du Viver et al., 2014) indicating that the global ocean basins were very well connected by this time and archive a synchronous termination at ~94.3 Ma of this interval of persistently intense volcanism. Given that this interval of inferred sustained volcanism occurred within the Stage C3 of the positive CIE, this supports a causal link between volcanism and the global carbon perturbation during the initiation of OAE2.

Toward the end of the interval of sustained volcanism, inferred from the 200 kyr interval of minimum Osi values, $\Delta^{13}C$ ($\delta^{13}C_{carb}$ — $\delta^{13}C_{org}$) reaches a minimum as well and is expressed as a three episodes of minima that together persist through substage C3c into the early stage C4 suggesting possible episodic short-term decreases in atmospheric pCO_2 (cf. Kump and Arthur, 1999; Jarvis et al., 2011). The total duration of this $\Delta^{13}C$ minima is estimated at ~120 kyr that we interpret to record a period of repeated short-term cooling (SM5). Given the time-scale of the fluctuations (10^4-yr), the short-lived decreases in pCO_2 were likely driven by increases in carbon sequestration through enhanced organic matter burial (e.g., Barclay et al., 2010) although the ~120 kyr overall duration could have been further influenced by increased CO_2 sequestration by greater silicate weathering (e.g., Clarkson et al., 2018). We posit that this inferred period of cooling may be the Southern Hemisphere counterpart of the Plenus Cold Event (PCE), which is widely recognized in the Northern Hemisphere (e.g., Gale and Christensen, 1996; Forster et al., 2007; Sinninghe Damsté et al., 2010; Jarvis et al., 2011; Jenkyns et al., 2017; O'Connor et al., 2020). In Europe, the PCE is indicated by the southward incursion of boreal fauna as documented in Plenus Marls in English chalk (e.g., Jefferies, 1962, 1963). The main phase of the PCE cooling spans the upper part of C isotope substage C3b to C3c and the $\Delta^{13}C$ minima are shown to generally straddle the substage C3b trough (Jarvis et al., 2011; Jenkyns et al., 2017; SM2). In contrast, the $\Delta^{13}C$ minima of the Tibetan section occurs later in substage C3c and the early part of the stage C4 (Fig. 2). If $\Delta^{13}C$ minima of the Tibetan section and the English chalk faithfully recorded the PCEs, these results would suggest a possible delay in the cooling in the Southern Hemisphere relative to the Northern Hemisphere. Within the Northern Hemisphere, recent analysis of multiple paleotemperature proxy data appears to show diachronous occurrence of the PCEs at an individual site that is related to local processes (O'Connor et al., 2020; Percival et al., 2020). The elevated $\Delta^{13}C$ values, toward the close of the CIE of the Tibetan section (Fig. 2) may indicate subsequent warming, which is consistent with the paleotemperature record from ODP1138 (Robinson et al., 2019). Notably, the two Southern Hemisphere records for OAE2 (the Tibetan section and ODP1138 core) do not support the hypothesis that termination of OAE2 resulted from cooling driven by enhanced sequestration of atmospheric CO_2 in response to large-scale organic C burial in the early stage of OAE2 (Arthur et al., 1988). Termination of OAE2 by orbital forcing of insolation (2.4 Myr orbital cycle) remains a viable mechanism by which ocean circulation and deep-water ventilation were enhanced (Li et al., 2017).

5) Implications

Consideration of all high-resolution Osi records available for highly expanded OAE2 intervals from sections or cores with good age constraints provides compelling evidence for volcanism-induced anoxia in the proto-North Atlantic Ocean perhaps beginning as early as ~94.8 Ma. Global onset of OAE2, however, did not begin until ~94.5 Ma coincident with a global transgression that we hypothesize increased the connectivity of the world's oceans and thus led to greater ocean ventilation, widespread distribution of warm saline water with low oxygen contents but rich in magmatic-sourced nutrients from the proto-North Atlantic basin (Hay et al., 1999). The concomitant expansion of the O_2-minimum zone with transgression (Thurow et al., 1992) would have had the potential to drive widespread ocean anoxia (e.g., van Helmond et al., 2014; Lowery et al., 2017). Nd isotopic records from the European continental sea document enhanced bottom water influence (Zheng et al., 2013, 2016) accompanied by the overall westward current of upper ocean water connecting the Tethys and North Atlantic (e.g., Bush, 1997; Pucéat et al., 2005), indicating a substantial change in the overturning ocean circulation rates that is considered critical for developing OAE2 (Arthur, 2018). Although the impact on long-term climate change through the late Cretaceous has long been recognized from climate simulations (e.g., Poulsen et al., 2001; Otto-Bliesner et al., 2002; Donnadieu et al., 2016; Ladant et al., 2020), the integration of OAE2 isotopic records from several well age-constrained sections and cores presented in this study provides strong evidence for the important role that increased ocean connectivity played in initiating the global but geologically brief OAE2. Today the surface oceans in the low-latitudes and many coastal regions are experiencing deoxygenation in response to global warming and likely future sea level rise (e.g., Keeling et al., 2010; Shepherd et al., 2017; Laffoley and Baxter, 2019). In that context, this study of OAE2, which occurred as one of several oceanic anoxic events under a greenhouse climate, highlights the importance of incorporating sensitivity tests of how changes in paleobathymetry (e.g., here volcanic sills) and sea level rise influence the connectivity between major ocean basins.

Acknowledgements

This research was supported by the National Natural Science Foundation of China (41774075, 41888101). We thank Prof. Brad Sageman for discussions related to sedimentary records recording transgressions in the late Cenomanian and Dr. Matt Jones for discussion of the correlation between the Portland core and the Iona-1 core, Dr. X-Y Zhen for discussion about ocean circulation with Nd isotope data. We thank Antonia Hofmann, Geoff Nowell, and Chris Ottley for assistance with Re-Os geochemical analyses. DS acknowledges funding from the TOTAL Endowment Fund and the CUG Wuhan Dida Scholarship. Lifeng Ma and Shipeng Wang are thanked for their field assistance.

Methods

In this study, we utilized fresh outcrop samples (N = 55) that were collected at a 10 to 20 cm spacing from the Gongzha OAE2 section and that were previously measured for magnetic susceptibility and carbon isotopes (Li et al., 2017). Each sample (~8 to 10 g) represents a ~2 cm stratigraphic interval. Thus, the samples used for this study are from the same stratigraphic level of those used for the high-resolution magnetic susceptibility and/or carbon isotope data in Li et al. (2017), thus eliminating any potential temporal uncertainties that could otherwise arise from stratigraphic offsets between different proxy records collected from independent sets of samples.

Individual samples were powdered in an agate mortar to homogenize the Re and Os within the sample (Kendall et al., 2009). The Re-Os analyses were performed in the geochemistry laboratory of Durham University, UK, following established analytical protocols (Selby and Creaser, 2003). In brief, 1 g homogenized sample powder and a known amount tracer solution, ^{190}Os + ^{185}Re, were loaded into a Carius tube, and were digested with 8 ml of CrO_3-H_2SO_4 solution in sealed Carius tubes. The Os was isolated using solvent extraction ($CHCl_3$) and purified with the microdistillation approach. The Re was isolated from the rhenium-bearing CrO_3-H_2SO_4 solution and purified using solvent extraction and anion chromatography. Isotope compositions of the purified Re and Os fractions were loaded onto nickel (for rhenium) and platinum (for osmium) filaments and measured using negative thermal ion mass spectrometry (NTIMS). Total procedural blanks during this study were 12.1 ± 2.5 pg and 0.10 ± 0.05 pg for Re and Os, respectively, with an average $^{187}Os/^{188}Os$ value of 0.25 ± 0.05 (1σ S.D, N = 8).

The samples for $\delta^{13}C_{org}$ measurement (N=75) were weighed into beakers and reacted with 2 mol/L HCl at room temperature for 24 hours. The treated samples were subsequently rinsed with DI water and dried on a heating plate at 50°C. The dried samples were combusted for at least 4 hours at 800-850°C and the CO_2 was purified and isolated by cryogenic distillation. Bulk organic matter $\delta^{13}C_{org}$ was measured on a MAT251 gas mass spectrometer with a dual inlet system at the Stable Isotope Geochemistry Lab in the Institute of Earth Environment, CAS. All results were reported to V-PDB and standard deviation is less than 0.3‰.

Author contributions

YXL led the project, performed stratigraphic correlation analysis, and wrote the draft of the paper; XYL conducted osmium isotope measurements of the majority of samples supervised by DS. DS measured the rest of samples for osmium isotopes, and contributed to Os data analysis, interpretation, and discussion. ZHL contributed to δ^{13}Corg data collection and discussion; IPM contributed to carbon isotope data interpretation and discussion; XHL contributed to stratigraphic analysis. All authors contributed to writing of the manuscript and its revision.

Data availability

The δ^{13}Corg data and the osmium isotope data of this study are presented in Table 1 and Table 2.

References

Arthur, M.A., Dean, W.E., Pratt, L.M., 1988. Geochemical and climatic effects of increased marine organic carbon burial at the Cenomanian/Turonian boundary. Nature 335, 714–717.

Arthur, M. A., Schlanger, S. O., and Jenkyns, H. C., 1987, The Cenomanian-Turonian Oceanic Anoxic Event, II. Palaeoceanographic controls on organic-matter production and preservation: Geological Society, London, Special Publications, 26(1), 401-420.

Arthur, M.A. 2018. The causes and consequences of Cretaceous oceanic anoxic events reconsidered. Goldschmidt 2018 Abstract

Barclay, R.S., McElwain, J.C., Sageman, B.B., 2010. Carbon sequestration activated by a volcanic CO2 pulse during Oceanic Anoxic Event 2. Nat. Geosci.3. 205–208, https://doi.org/10.1038/NGEO757.

Beil, S., Kuhnt, W., Holbourn, A.E., Aquit, M., Flögel, S., Challai, E.H., Jabour, H., 2018. New insights into Cenomanian paleoceanography and climate evolution from the Tarfaya Basin, southern Morocco. Cretaceous Research 84, 451-473.

Blakey, 2011 Global paleogeography. NAU Geology. http://jan.ucc.nau.edu/~rcb7/globaltext2.html

Blättler, C.L., Jenkyns, H. C., Reynard, L.M., Henderson, G.M., 2011. Significant increases in global weathering during Oceanic Anoxic Events1a and 2 indicated by calcium isotopes. Earth Planet. Sci. Lett. 309, 77–88.

Bralower, T.J., 2008. Volcanic cause of catastrophe. Nature 454, 285–287.

Bush, A.B.G., 1997. Numerical simulation of the Cretaceous Tethys Circum global Current. Science 275, 807–810.

Clarkson, M.O, Stirling, C.H., Jenkyns, H.C., Dickson, A.J., Porcelli, D. et al., 2018. Uranium isotope evidence for two episodes of deoxygenation during Oceanic Anoxic Event 2. PNAS 115 (12), 2918-2923.

Donnadieu, Y., Pucéat, E., Moiroud, M., Guillocheau, F., Deconinck, J-F., 2016. A better-ventilated ocean triggered by Late Cretaceous changes in continental configuration. Nature Communications, doi: 10.1038/ncomms10316.

Du Vivier, A.D.C., Selby, D., Sageman, B.B., Jarvis, I., Gröcke, D.R., Voigt, S., 2014. Marine 187Os/188Os isotope stratigraphy reveals the interaction of volcanism and ocean circulation during Oceanic Anoxic Event 2. Earth Planet. Sci. Lett. 389, 23–33.

Du Vivier, A., D. Selby, D., Condon, D.J., Takashima, R. and Nishi, H., 2015 Pacific $^{187}Os/^{188}Os$ isotopic chemistry and U–Pb geochronology: synchroneity of global Os isotope change across OAE 2. Earth Planet. Sci. Lett., 428, 204–216.

Eldrett, J. S., Ma, C., Bergman, S. C., Lutz, B., Gregory, F. J., Dodsworth, P., Phipps, M., Hardas, P., Minisini, D., Ozkan, A., Ramezani, J., 2015. An astronomically calibrated stratigraphy of the Cenomanian, Turonian and earliest Coniacian from the Cretaceous Western Interior Seaway, USA: Implications for global chronostratigraphy, Cretaceous Res., 56, 316–344.

Eldrett, J. S., Dodsworth, P., Bergman, S. C., Wright, M., Minisini, D., 2017. Water-mass evolution in the Cretaceous Western Interior Seaway of North America and equatorial Atlantic. Climate of the Past, 13, 855–878.

Elrick, M., Molina-Garza, R., Duncan, R., Snow, L., 2009. C-isotope stratigraphy and paleoenvironmental changes across OAE2 (mid-Cretaceous) from shallow-water platform carbonates of southern Mexico. Earth and Planetary Science Letters, 277(3-4), 295–306. https://doi.org/10.1016/j.epsl.2008.10.020

Forster, A., Schouten, S., Moriya, K., Wilson, P. A., Sinninghe Damsté, J. S., 2007.

Tropical warming and intermittent cooling during the Cenomanian/Turonian oceanic anoxic event 2: Sea surface temperature records from the equatorial Atlantic. Paleoceanography, 22(1), PA1219. https://doi.org/10.1029/2006pa001349

Gale, A.S., Voigt, S., Sageman, B.B. and Kennedy, W.J., 2008. Eustatic sea-level record for the Cenomanian (Late Cretaceous)−−Extension to the Western Interior Basin, USA. Geology 36, 859-862.

Gale, A. S., and Christensen, W. K., 1996. Occurrence of the belemnite Actinocamax plenus in the Cenomanian of SE France and its significance. Bulletin of the Geological Society of Denmark, 43(1), 68–77.

Gambacorta, G., Jenkyns, H.C., Russo, F., Tsikos, H., Wilson, P.A. and Erba, E. 2015. Carbon- and oxygen isotope records of mid-Cretaceous Tethyan pelagic sequences from the Umbria–Marche and Belluno Basins (Italy). Newsl. Stratigr., 48, 299–323

Gomes, M.L., Hurtgen, M.T. and Sageman, B.B., 2016. Biogeochemical sulfur cycling during cretaceous ocean anoxic events: a comparison of OAE1a and OAE2. Paleoceanography, 31, 233–251.

Haq, B. U., 2014. Cretaceous eustasy revisited: Global and Planetary Change 113, 44–58.

Hay, W.W., DeConto, R.M., Wold, C.N., Wilson, K.M., Voigt, S., Schulz, M., Wold, A.R., Dullo, W.-Chr., Ronov, A.B., Balukhovsky, A.N., Söding, E., 1999. An alternative global Cretaceous paleogeography. In: Barrera, E., Johnson, C.C. (Eds.), Evolution of the Cretaceous Ocean-Climate System. Geological Society of America Special Paper 332, 1–47.

Hay, W. W., 2008. Evolving ideas about the Cretaceous climate and ocean circulation. Cretaceous Research 29, 725–753.

van Helmond, N. A. G. M., I. Ruvalcaba Baroni, A. Sluijs, J. S. Sinninghe Damsté, C. P. Slomp, 2014. Spatial extent and degree of oxygen depletion in the deep proto-North Atlantic basin during Oceanic Anoxic Event 2, Geochem. Geophys. Geosyst., 15, 4254–4266, doi:10.1002/2014GC005528.

Jarvis, I., Lignum, J.S., Gröcke, D.R., Jenkyns, H.C., 2011. Pearce MA Black shale deposition, atmospheric CO2drawdown and cooling during the Cenomanian–Turonian Oceanic Anoxic Event. Paleoceanography 26, PA3201. http://dx.doi.org/10.1029/2010PA002081.

Jefferies, R. P. S., 1962. The paleoecology of the Actinocamax plenus subzone (lowest Turonian) in the Anglo-Paris Basin. Paleontology, 4(4), 609–647.

Jefferies, R. P. S., 1963. The stratigraphy of the Actinocamax plenus Subzone (Turonian) in the Anglo-Paris Basin. Proceedings of the Geologists' Association, 74(1), 1–33. https://doi.org/10.1016/s0016-7878(63)80011-5

Jenkyns, H. C., A. Matthews, H. Tsikos, Y. Erel, 2007. Nitrate reduction, sulfate reduction, and sedimentary iron isotope evolution during the Cenomanian - Turonian oceanic anoxic event, Paleoceanography, 22, PA3208, doi:10.1029/2006PA001355.

Jenkyns, H.C., 2010. Geochemistry of oceanic anoxic events. Geochem. Geophys. Geosyst. 11, Q03004.

Jenkyns, H.C., Dickson, A.J., Ruhl, M., van den Boorn, S.H.J.M., 2017, Basalt–seawater interaction, the Plenus Cold Event, enhanced weathering and geochemical change: deconstructing Oceanic Anoxic Event 2 (Cenomanian–Turonian, Late Cretaceous). Sedimentology 64, 16–43.

Jones, M. M., Sageman, B. B., Oakes, R. L., Parker, A. L., Leckie, R. M., Bralower, T. J., Sepúlveda, J., and Fortiz, V., 2019. Astronomical pacing of relative sea level during Oceanic Anoxic Event 2: Preliminary studies of the expanded SH#1 Core, Utah, USA, GSA Bulletin, 131, (9-10), 1702-1722, https://doi.org/10.1130/B32057.1.

Jones, M. M., Sageman, B. B., Selby, D., Jichad, B.R., Singer, B. S. 2020. Regional chronostratigraphic synthesis of the Cenomanian-Turonian Oceanic Anoxic Event 2 (OAE2) interval, Western Interior Basin (USA): New Re-Os chemostratigraphy and $^{40}Ar/^{39}Ar$ geochronology. Geological Society of America Bulletin. doi: https://doi.org/10.1130/B35594.1

Keeling, R. E., Kortzinger, A., Gruber, N., 2010. Ocean deoxygenation in a warming world. Annual Review of Marine Science 2, 199–229.

Kendall, B., Creaser, R. A., and Selby, D., 2009, 187Re-187Os geochronology of Precambrian organic-rich sedimentary rocks. Geol. Soc. London Spec. Pub. 326, 85-107.

Kuhnt, W., Holbourn, A.E., Beil, S., Aquit, M., Krawczyk, T., Flögel, S., Chellai, E.H., Jabour, H., 2017. Unraveling the onset of Cretaceous Oceanic Anoxic Event 2 in an extended sediment archive from the Tarfaya-Laayoune Basin, Morocco. Paleoceanography 32, 923–946. https://doi.org/10.1002/2017PA003146.

Kump, L.R., Arthur, M.A., 1999. Interpreting carbon-isotope excursions: carbonate and organic matter. Chem. Geol.161, 181–198. http://dx.doi.org/10.1016/S0009-2541(99)00086-8.

Laffoley, D., Baxter, J.M., (eds.) 2019. Ocean deoxygenation: Everyone's problem - Causes, impacts, consequences and solutions. Full report. Gland, Switzerland: IUCN. 580pp.

Ladant, J-B., Poulsen, C.J., Fluteau, F., Tabor, C.R., MacLeod, K.G., Martin, E.E., Haynes, S.J., Rostami, M.A., 2020. Paleogeographic controls on the evolution of Late Cretaceous ocean circulation. Clim. Past, 16, 973–1006, https://doi.org/10.5194/cp-16-973-2020

Larson, R. L., 1991. Geologic consequences of superplumes. Geology, 19(10), 963–966.

Li, X.H., Jenkyns, H.C., Wang, C.S., Hu, X.M., Chen, X., Wei, Y.S., Huang, Y.J., Cui, J., 2006. Upper Cretaceous carbon and oxygen isotope stratigraphy of hemipelagic carbonate facies from southern Tibet, China. J. Geol. Soc. Lond. 163, 375–382.

Leckie, R.M., Bralower, T.J., Cashman, R., 2002. Oceanic anoxic events and plankton evolution: biotic response to tectonic forcing during the mid-Cretaceous. Paleoceanography 17, 623–642.

Li, Y. X., Montañez, I. P., Liu, Z. H., and Ma, L. F., 2017, Astronomical constraints on global carbon-cycle perturbation during Oceanic Anoxic Event 2 (OAE2). Earth and Planetary Science Letters. 462, 35-46.

Lowery, C. M., Cunningham, R., Barrie, C. D., Bralower, T., Snedden, J. W., 2017. The northern Gulf of Mexico during OAE2 and the relationship between water depth and black shale development. Paleoceanography, 32, 1316–1335. https://doi.org/10.1002/2017PA003180

Mahoney, J. J., M. Storey, R. A. Duncan, K. J. Spencer, and M. Pringle, Geochemistry and age of the Ontong Java Plateau, in *The Mesozoic Pacific: Geology, Tectonics, and Volcanism*, Geophys. Monogr. Ser., vol. 77, edited by M. Pringle et al., pp. 233 – 261, AGU, Washington, D.C., 1993.

Meyers, S.R., Siewert, S.E., Singer, B.S., Sageman, B.B., Condon, D.J., Obradovich, J.D., Jicha, B.R., Sawyer, D.A., 2012. Intercalibration of radioisotopic and astrochronologic time scales for the Cenomanian–Turonian boundary interval, Western In-terior Basin, USA. Geology 40, 7–10.

Navarro-Ramirez, J.P., Bodin, S. and Immenhauser, A., 2016. Ongoing Cenomanian — Turonian heterozoan carbonate production in the neritic settings of Peru. Sedimentary Geolody 331, 78-93.

O'Connor, L.K., Jenkyns, H.C., Robinson, S.A., Remmelzwaal, S.R., Batenburg, S.J., Parkinson, I.J., Gale, A.S., 2020. A re‐evaluation of the Plenus Cold Event, and the links between CO2, temperature, and seawater chemistry during OAE 2. Paleoceanography and Paleoclimatology, 35, https://doi.org/10.1029/2019PA003631.

Otto-Bliesner, B. L., Brady, E. C., Shields, C., 2002. Late Cretaceous ocean: Coupled simulations with the National Center for Atmospheric Research Climate System Model, J. Geophys. Res., 107, ACL-11, https://doi.org/10.1029/2001jd000821.

Owens, J. D., Gill, B.C., Jenkyns, H.C., Bates, S.M., Severmann, S., Kuypers, M.M.M., Woodfine, R.G., Lyons, T.W., 2013. Sulfur isotopes track the global extent and dynamics of euxinia during Cretaceous Oceanic Anoxic Event 2. PNAS 110, 18407–18412.

Oxburgh, R., 2001. Residence time of osmium in the oceans. Geochem. Geophys. Geosyst .2.2000GC00010.

Percival, L.M.E., van Helmond, N.A.G.M., Selby, D., Goderis, S., Claeys, P. 2020 (in press). Complex interactions between large igneous province emplacement and global temperature changes during the Cenomanian–Turonian oceanic anoxic event (OAE 2). Paleoceanography and Paleoclimatology, doi: 10.1029/2020PA004016

Pogge von Strandmann, P.A.E., Jenkyns, H.C., Woodfine, R.G., 2013. Lithium isotope evidence for enhanced weathering during Oceanic Anoxic Event 2. Nat. Geosci. 6, 668–672.

Poulsen, C. J., Barron, E. J., Arthur, M. A., Peterson, W. H. 2001. Response of the Mid-Cretaceous global oceanic circulation to tectonic and CO_2 forcings, Paleoceanography 16, 576–592, https://doi.org/10.1029/2000pa000579.

Pucéat, E., Lécuyer, C., Reisberg, L., 2005. Neodymium isotope evolution of NW Tethyan upper ocean waters throughout the Cretaceous. Earth Planet. Sci. Lett. 236, 705–720, doi:10.1016/j.epsl.2005.03.015.

Richardt, N., Wilmsen, M., Niebuhr, B., 2013. Late Cenomanian–Early Turonian facies development and sea-level changes in the Bodenwöhrer Senke (Danubian Cretaceous Group, Bavaria, Germany). Facies (2013) 59, 803–827. doi: 10.1007/s10347-012-0337-x

Robinson, S. A., Dickson, A. J., Pain, A., Jenkyns, H. C., O'Brien, C. L., Farnsworth, A., Junt, D. L., 2019. Southern Hemisphere sea-surface temperatures during the Cenomanian-Turonian: Implications for the termination of Oceanic Anoxic Event 2. Geology 47, 131–134.

Rooney, A.D., D. Selby, J.M. Lloyd, D.H. Roberts, A. Lückge, B.B. Sageman, N.G. Prouty, 2016. Tracking millennial-scale Holocene glacial advance and retreat using osmium isotopes: insights from the Greenland Ice Sheet. Quatern. Sci. Rev., 138, 49-61, doi:10.1016/j.quascirev.2016.02.021

Sageman, B.B., Meyers, S.R., Arthur, M.A., 2006. Orbital time scale and new C-isotope record for Cenomanian–Turonian boundary stratotype. Geology 34, 125–128. http://dx.doi.org/10.1130/G22074.1.

Schlanger, S.O., Jenkyns, H.C., 1976. Cretaceous oceanic anoxic events: causes and consequences. Geol. Mijnb. 55, 179–184.

Selby, D., Creaser, R.A., 2003. Re–Os geochronology of organic rich sediments: An evaluation of organic matter analysis methods. Chem. Geol. 200, 225–240.

Shepherd, J.G., Brewer, P.G., Oschlies, A., Watson, A.J., 2017. Ocean ventilation and deoxygenation in a warming world: introduction and overview. Phil. Trans. R. Soc. A 375: 20170240. http://dx.doi.org/10.1098/rsta.2017.0240

Sinninghe Damsté, J. S., van Bentum, E. C., Reichart, G.J., Pross, J., Schouten, S. 2010. A CO_2 decrease-driven cooling and increased latitudinal temperature gradient during the mid-Cretaceous Oceanic Anoxic Event 2. Earth Planet. Sci. Lett. 293(1-2), 97–103. https://doi.org/10.1016/j.epsl.2010.02.027

Sullivan, D.L., Brandon, A.D., Eldrett, J., Bergman, S.C., Wright, S., Minisini, D., 2020. High resolution osmium data record three distinct pulses of magmatic activity during Cretaceous oceanic anoxic event 2 (OAE-2), Geochimica et Cosmochimica Acta, doi: https://doi.org/10.1016/j.gca.2020.04.002

Snow, L.J., Duncan, R.A., Bralower, T.J., 2005. Trace element abundances in the Rock Canyon Anticline, Pueblo, Colorado, marine sedimentary section and their re-lationship to Caribbean plateau construction and oceanic anoxic event 2. Paleoceanography 20, PA3005.

Takashima, R., Nishi, H., Yamanaka, T., Tomosugi, T., Fernando, A.G., Tanabe, K., Moriya, K., Kawabe, F., Hayashi, K., 2011. Prevailing oxic environments in the Pacific Ocean during the mid-Cretaceous Oceanic Anoxic Event 2. Nat. Commun. 2, 234.

Tegner, C., Storey, M., Holm, P.M., Thorarinsson, S.B., Zhao, X., Lo, C.-H., Knud-sen, M.F., 2011. Magmatism and Eurekan deformation in the High Arctic Large Igneous Province: ^{40}Ar–^{39}Ar age of Kap Washington Group volcanics, North Greenland. Earth Planet. Sci. Lett. 303, 203–214.

Thurow, J., Brumsak, H.-J., Rullkotter, J., Littke, R., Meyers, P., 1992. The Cenomanian-Turonian boundary event in Indian Ocean-a key to understand the global picture. Geophysical Monograph 70, AGU.

Tsikos, H., Jenkyns, H.C., Walsworth-Bell, B., Petrizzo, M.R., Forster, A., Kolonic, S., Erba, E., Premoli Silva, I., Baas, M., Wagner, T., Sinninghe Damsté, J.S., 2004.

Carbon-isotope stratigraphy recorded by the Cenomanian–Turonian oceanic anoxic event; correlation and implications based on three key localities. J. Geol. Soc. Lond.161, 711–719.

Turgeon, S.C., Creaser, R.A., 2008. Cretaceous oceanic anoxic event 2 triggered by a massive magmatic episode. Nature 454, 323–326.

van Helmond, N. A. G. M., I. Ruvalcaba Baroni, A. Sluijs, J. S. Sinninghe Damsté, C. P. Slomp, 2014. Spatial extent and degree of oxygen depletion in the deep proto-North Atlantic basin during Oceanic Anoxic Event 2, Geochem. Geophys. Geosyst., 15, 4254–4266, doi:10.1002/2014GC005528.

Voigt, S., Gale, A.S., Voigt, T., 2006. Sea-level changes, carbon cycling and palaeoclimate during the Late Cenomanian of northwest Europe; an integrated palaeoenvironmental analysis. Cretaceous Research 27, 836–858

Wang, C. S., Hu, X.M., Huang, Y.J., Wagreich, M., Scott, R., Hay, W., 2011. Cretaceous oceanic red beds as possible consequence of oceanic anoxic events. Sediment. Geol. 235, 27–37.

Wu, H.C., Zhang, S.H., Jiang, G.Q., Huang, Q.H., 2009. The floating astronomical time scale for the terrestrial Late Cretaceous Qingshankou Formation from the Songliao Basin of Northeast China and its stratigraphic and paleoclimate implications. Earth Planet. Sci. Lett. 278, 308–323.

Zheng, X.-Y., Jenkyns, H.C., Gale, A.S., Ward, D.J., Henderson, G.M., 2013. Changing ocean circulation and hydrothermal inputs during Ocean Anoxic Event 2 (Cenomanian–Turonian): Evidence from Nd-isotopes in the Euro-pean shelf sea. Earth Planet. Sci. Lett. 375, 338–348.

Zheng, X.-Y., Jenkyns, H.C., Gale, A.S., Ward, D.J., Henderson, G.M., 2016. A climatic control on reorganization of ocean circulation during the mid-Cenomanian event and Cenomanian–Turonian oceanic anoxic event (OAE 2): Nd isotope evidence. Geology 44, 151 – 154.

Figure captions

Fig. 1 Paleogeographic map (~90 Ma) showing the locations of major OAE2 sections.

The Gongzha (GZ) section, southern Tibet of this study is marked by a purple circle. Other sections where Os isotope data are reported are shown by yellow circles (data from Turgeon and Creaser, 2008; Du Vivier et al., 2014, 2015; Sullivan et al., 2020; Percival et al., 2020) and the underlined labels (P, Iona-1, YG and GZ) indicate the locations of OAE2 sections that exhibit high-resolution correlation in Fig. 3. Sites that document the late Cenomanian transgressions are shown by yellow stars (data from Voigt et al., 2006; Gale et al., 2008; Navarro-Ramirez et al., 2016; Beil et al., 2018). 530A – Site 530A, Angola Basin. 1260 – Site 1260 B, Demerara Rise, Atlantic Ocean. E – Eastbourne, UK. F – Furlo, Italy. GVS – Great Valley Sequence, California, USA. G – Grböern, Germany. Iona-1 – Shell Iona-1, Texas, USA. P – USGS Portland #1 Core, Colorado, USA. PU – Pueblo, Colorado, USA. 174AX – Bass River, New Jersey Shelf, USA. T – Tarfaya Basin, Morocco. VB – Vocontian Basin, Italy. W – Wunstorf, Germany. WP – Western Platform, Peru. YG – Yezo Group, Hokkaido, Japan. CP, Caribbean Plateau; HALIP, High Arctic Large Igneous Province; KP, Kerguelen Plateau. Paleogeographic reconstruction was modified from Blakey (2011).

Fig. 2 The integrated stratigraphy of Cenomanian/Turonian Boundary (CTB) succession in Gongzha, Tingri, southern Tibet. The bio- and lithostratigraphy (a) (Li et al., 2006), cyclostratigraphy (b), and the high-resolution carbon isotope stratigraphy (c) with carbon isotope stages C2 through C5 marked with different color bands are from Li et al. (2017). (d) The Osmium isotope stratigraphy and (e) organic carbon isotope stratigraphy, along with $\Delta^{13}C$ data (f), of this study. The asterisk marks the recently refined CTB age of 93.95±0.05 Ma (Jones et al., 2020) from 93.9±0.15 Ma (Meyers et al., 2012). The CTB was previously anchored at the C4/C5 boundary (Li et al., 2017) and thus is updated by anchoring the CTB at a half short eccentricity cycle, i.e., ~50 kyr, below the C4/C5 boundary (Fig. S1-1). This update does not affect numerical age estimates for carbon isotope stage boundaries. For instance, the age of the C4/C5 boundary remains at ~93.9 Ma. The numbers in red indicate the estimated ages for the three Osi shifts using the anchored orbital timescale in (b). The red arrows in (f) mark the three Osi excursions; The orange arrows in (d) indicate major inflection points in the $\delta^{13}C_{org}$ curve; The dashed curve in (e) indicates the interval of low $\Delta^{13}C$, representing episodic cooling.

Fig. 3 The osmium isotope data of four representative OAE2 sections show the striking similarity of the Osi variations across the CTB interval and the different phasing relationship between Osi excursions and the onset of OAE2. Color bands indicate different carbon isotope stages of OAE2 (c) that are used to establish correlations of the OAE2 records. The ages and durations of these carbon isotope stages are constrained with the significantly expanded OAE2 record from the Gongzha section in southern Tibet (Fig. 2). (a) The Portland #1 core, WIS (Sageman et al., 2006; Meyers et al., 2012; Du Vivier et al., 2014); (b) The Iona-1 Core, WIS (Eldrett et al., 2015; Sullivan et al., 2020); (c) the Gongzha section, southern Tibet (Li et al., 2017; this study); (d) The Yezo Group, Japan (Takashima et al., 2011; Du Vivier et al., 2015). Syn. ending, synchronous ending of the episode of intensified volcanism; E.E. volcanism, earlier episode of volcanism. C3a' is the defined CIE prior to the globally correlative CIE in the Iona-1 core and is considered to represent regional CIE during restricted ocean conditions. See text for discussion. See Fig. S2-1 for the common age-scale correlation of these sections. The vertical blue bars in (a), (b), (c) mark the inferred cooling interval of the Plenus Cold Event (PCE): (a) is based on Pervical et al (2020), (b) is based on correlation with the English chalk (Jenkyns et al., 2017; O'connor et al., 2020), (c) is based on Fig. 2 of this study.

Fig. 4 The OAE2 sections that document a transgression during the perturbation stage (C3) of OAE2. These sections are from the circum proto-North Atlantic basin and the transgression can be broadly correlated. The arrows mark the stratigraphic level of transgressive surface (TS). The pink bands indicate the perturbation stage C3 of OAE2. See Fig. 1 for locations of these sections.

Table captions

Table 1 The $\delta^{13}C_{org}$ data of the OAE2 interval in Gongzha section, southern Tibet, China

Table 2 Re-Os isotope data of the OAE2 interval in Gongzha section, southern Tibet, China

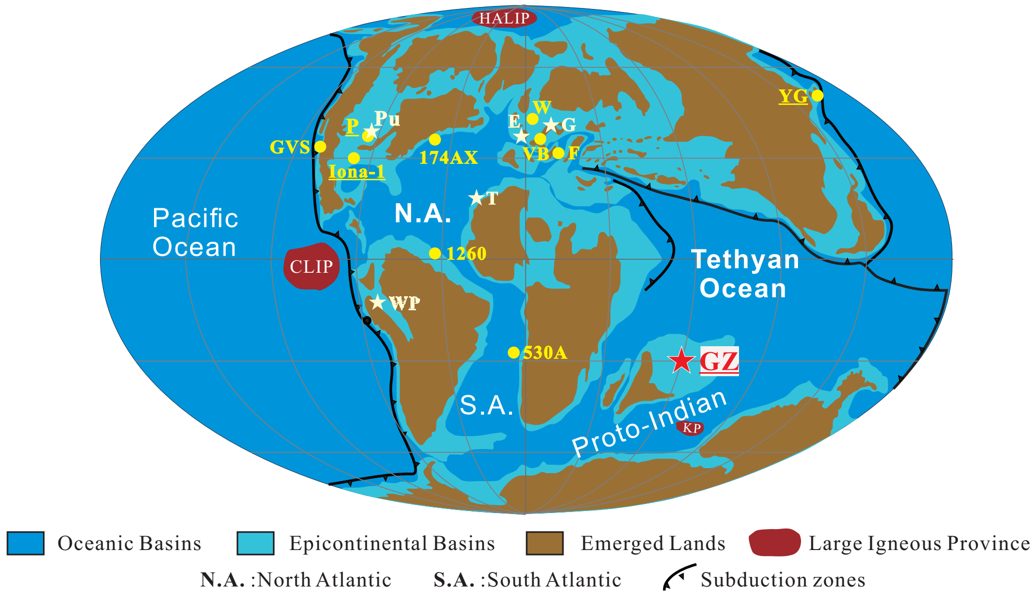

Fig. 1 Paleogeographic map (~90 Ma) showing the locations of major OAE2 sections. The Gongzha (GZ) section, southern Tibet of this study is marked by a red star. Other sections where Os isotope data are shown by yellow circles (data from Turgeon and Creaser, 2008; Du Vivier et al., 2014, 2015; Sullivan et al., 2020; Pervical et al., 2020) and the underlined labels (P, Iona-1, YG, and GZ) indicate the locations of OAE2 sections that exhibit high-resolution correlation in Fig. 3. Sites that document the late Cenomanian transgressions are shown by white stars (data from Voigt et al., 2006; Gale et al., 2008; Navarro-Ramirez et al., 2016; Beil et al., 2018). 530A – Site 530A, Angola Basin. 1260 – Site 1260 B, Demerara Rise, Atlantic Ocean. E – Eastbourne, UK. F – Furlo, Italy. GVS – Great Valley Sequence, California, USA. G – Grböern, Germany. Iona-1 – Shell Iona-1, Texas, USA. P – USGS Portland #1 Core, Colorado, USA. PU – Pueblo, Colorado, USA. 174AX – Bass River, New Jersey Shelf, USA. T – Tarfaya Basin, Morocco. VB – Vocontian Basin, Italy. W – Wunstorf, Germany. WP – Western Platform, Peru. YG – Yezo Group, Hokkaido, Japan. CP, Caribbean Plateau. HALIP, High Arctic Large Igneous Province. KP, Kerguelen Plateau. Paleogeographic reconstruction was modified from Blakey(2011).

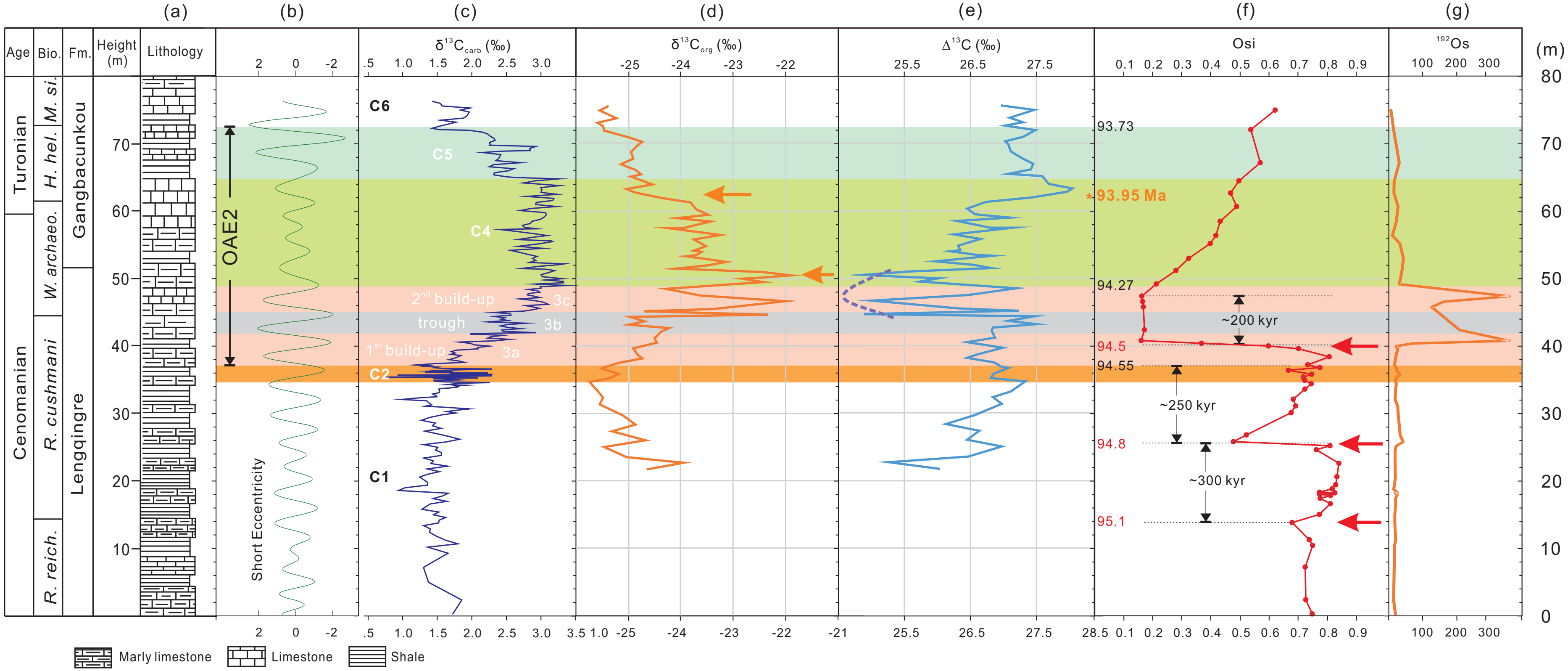

Fig. 2 The integrated stratigraphy of Cenomanian/Turonian Boundary (CTB) succession in Gongzha, Tingri, southern Tibet. The bio- and lithostratigraphy (a) (Li et al., 2006), cyclostratigraphy (b), and the high-resolution carbon isotope stratigraphy (c) with carbon isotope stages C2 through C5 marked with different color bands are from Li et al. (2017). (d) The Osmium isotope stratigraphy and (e) organic carbon isotope stratigraphy, along with $\Delta^{13}C$ data (f), of this study. The asterisk marks the recently refined CTB age of 93.95±0.05 Ma (Jones et al., 2020) from 93.9±0.15 Ma (Meyers et al., 2012). The CTB was previously anchored at the C4/C5 boundary (Li et al., 2017) and thus is updated by anchoring the CTB at a half short eccentricity cycle, i.e., ~50 kyr, below the C4/C5 boundary (Fig. S1-1). This update does not affect numerical age estimates for carbon isotope stage boundaries. For instance, the age of the C4/C5 boundary remains at ~93.9 Ma. The numbers in red indicate the estimated ages for the three Osi shifts using the anchored orbital timescale in (b). The red arrows in (f) mark the three Osi excursions; The orange arrows in (d) indicate major inflection points in the $\delta^{13}C_{org}$ curve; The dashed curve in (e) indicates the interval of low $\Delta^{13}C$, representing episodic cooling.

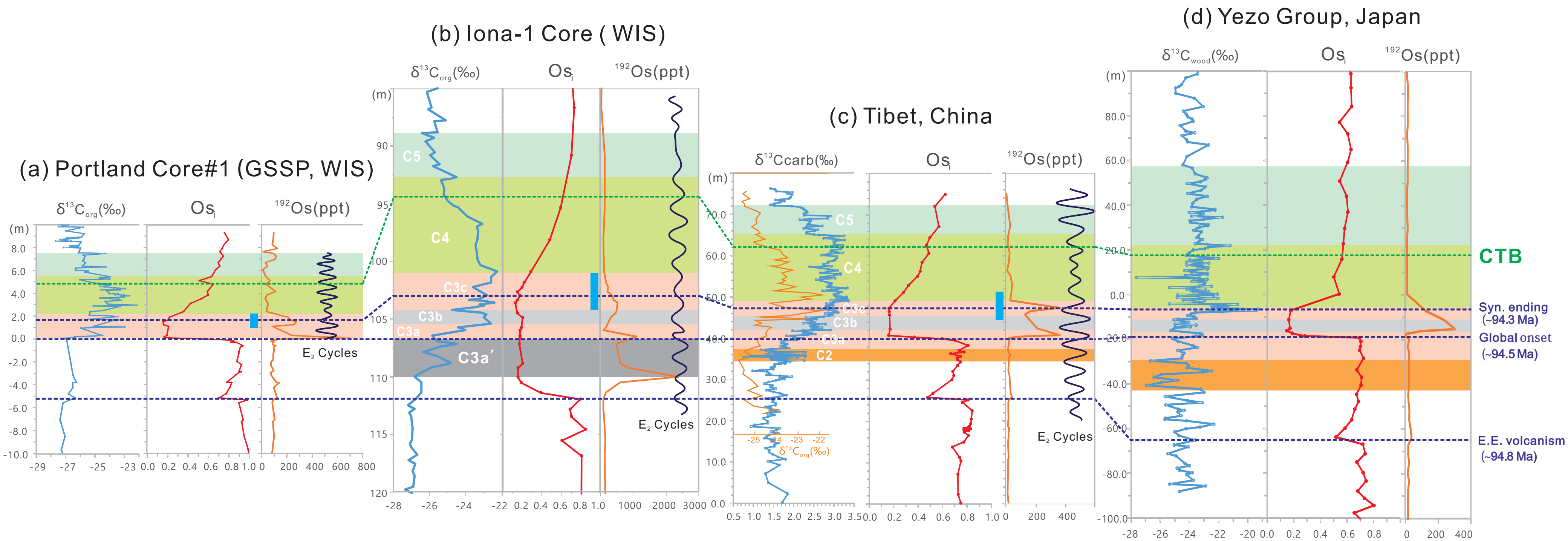

Fig. 3 The osmium isotope data of four representative OAE2 sections show the striking similarity of the Osi variations across the CTB interval and the different phasing relationship between Osi excursions and the onset of OAE2. Color bands indicate different carbon isotope stages of OAE2 (c) that are used to establish correlations of the OAE2 records. The ages and durations of these carbon isotope stages are constrained with the significantly expanded OAE2 record from the Gongzha section in southern Tibet (Fig. 2). (a) The Portland #1 core, WIS (Sageman et al., 2006; Meyers et al., 2012; Du Vivier et al., 2014); (b) The Iona-1 Core, WIS (Eldrett et al., 2015; Sullivan et al., 2020); (c) the Gongzha section, southern Tibet (Li et al., 2017; this study); (d) The Yezo Group, Japan (Takashima et al., 2011; Du Vivier et al., 2015). Syn. ending, synchronous ending of the episode of intensified volcanism; E.E. volcanism, earlier episode of volcanism. C3a' is the defined CIE prior to the globally correlative CIE in the Iona-1 core and is considered to represent regional CIE during restricted ocean conditions. See text for discussion. See Fig. S2-1 for the common age-scale correlation of these sections. The vertical blue bars in (a),(b),(c) mark the inferred cooling interval of the Plenus Cold Event (PCE): (a) is based on Pervical et al (2020), (b) is based on correlation with the English chalk (Jenkyns et al., 2017; O'connor et al., 2020), (c) is based on Fig. 2 of this study.

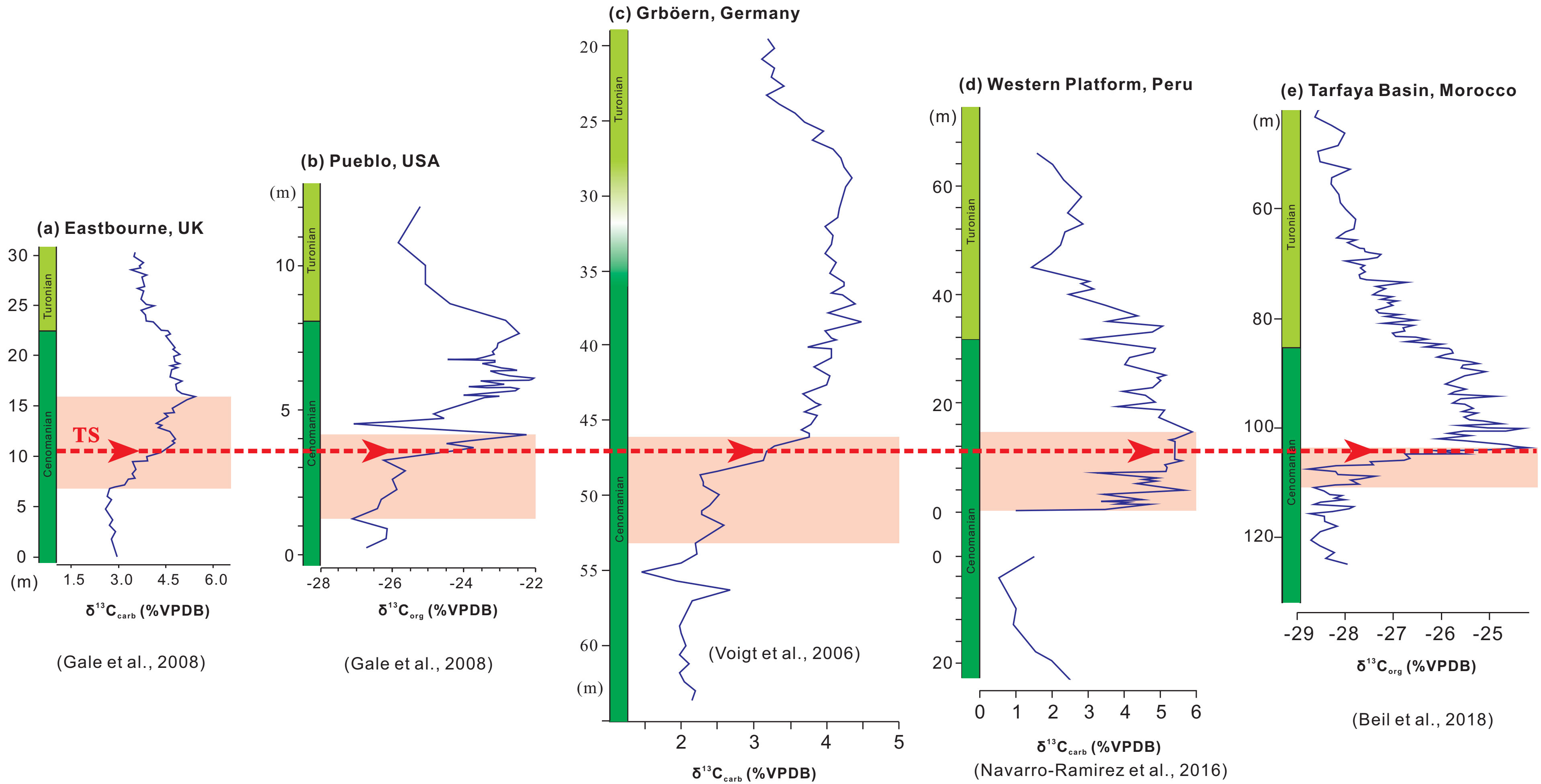

Fig. 4 The OAE2 sections that document a transgression during the perturbation stage (C3) of OAE2. These sections are from the circum proto-North Atlantic basin and the transgression can be broadly correlated. The arrows mark the stratigraphic level of transgressive surface (TS). The pink bands indicate the perturbation stage C3 of OAE2. See Fig. 1 for locations of these sections.